This is the pre-print version of the paper:

A. Alongi, A. Angelotti, L. Mazzarella, **Experimental investigation of the steady state behaviour of Breathing Walls by means of a novel laboratory apparatus**, Building and Environment 123 (2017) 415-426, http://dx.doi.org/10.1016/j.buildenv.2017.07.013

Experimental investigation of the steady state behaviour of Breathing Walls by means of a novel laboratory apparatus

A. Alongi[a], A. Angelotti[a,*], L. Mazzarella[a]

[a] *Politecnico di Milano, Department of Energy, Via Lambruschini, 4 (20156) Milano, Italy*

Abstract

Breathing Walls are envelope components, based on porous materials, crossed by a natural or forced airflow. Since they behave both as recovery heat exchangers and active insulation, reducing the conductive heat flux, they represent a promising envelope technology, allowing to reduce energy consumption in buildings.

From the modeling point of view, an analytical model can be found in literature, describing heat and mass transfer across Breathing Walls in steady state conditions. However, to the best of the authors' knowledge, the model lacks an exhaustive experimental validation. Therefore, in this paper, the novel laboratory apparatus named Dual Air Vented Thermal Box developed at Politecnico of Milano is presented. The apparatus is used to experimentally investigate the steady state behavior of a 1 m^2 Air Permeable Concrete sample, crossed by an airflow at different velocities up to 12 mm/s.

The temperature profile inside the sample, measured in different positions, is compared with the model predictions. While in the central portion of the wall a very good agreement is found, the experimental results at the top and at the bottom of the wall suggest a non-uniform velocity field entering the sample. A qualitative confirmation of this hypothesis is provided by CFD simulations on the apparatus, clearly showing a mixed convection regime on both sides of the wall. The results lead to state the validity of the one-dimensional analytical model in literature, although a careful application should take into account adjusted boundary conditions, consisting in an airflow velocity possibly variable with height.

Keywords: air permeable concrete, breathing wall, dynamic insulation, experimental assessment, laboratory apparatus

1. Introduction

In buildings with conventional envelopes, ventilation is either due to the operation of the windows or to the mechanical system. Airflows through the opaque constructions are basically uncontrolled and referred to as infiltrations. Conversely, in air permeable envelopes, porous materials such as pervious concrete, mineral wool or cellulose are used to compose the so called Breathing Walls and Roofs (also known as Dynamic Insulation). The overall stratigraphy usually consists of an external cladding, a ventilated air gap, a multi-layer porous core, a second air gap and an internal wearing surface [1]. If a small pressure difference is established either naturally or mechanically through the breathing component, a low velocity airflow is driven across it and the wall acts also as a ventilation system component.

Heat flux and air mass flow can either happen in opposite directions (*contra-flux* operation) or in the same (*pro-flux* operation). Most studies and applications focus on the contra-flux operation, that in heating dominated conditions allows to reduce the heat losses [2]. In such a configuration, the wall can also operate as an air filter towards outdoor particulate [3]. Moreover some authors [4] also pointed out the advantages of the pro-flux operation, that in warm climates, coupled with night free cooling, allows to enhance heat dissipation from the building. An original use of the Breathing Wall technology is proposed by [5] in a test building in Japan, where a part of the envelope is used in contra-flux, providing pre-heated fresh air to an indoor space, and another part is used in pro-flux, recovering heat from the exhaust air and storing it into the wall. Intake and ex-

*Corresponding author. Tel. 02 2399 5183; Fax. 02 2399 3913
Email address: adriana.angelotti@polimi.it
(A. Angelotti)

Nomenclature

A	analytical model characteristic parameter [m^{-1}]
c_p	specific heat at constant pressure [J/(kg·K)]
E	temperature control error [°C]
K_p	proportional gain [V/°C]
L	wall thickness [m]
P	pressure [Pa]
t	time [s]
T	temperature [°C]
$\mathbf{u}, u$	air velocity across the wall [m/s]
x	position [m]

Greek symbols

ε	volume fraction of fluid phase (porosity) [-]
λ	thermal conductivity [W/(mK)]
ρ	density [kg/m^3]
σ	standard deviation of a quantity [-]

Subscripts

c	characteristic quantity
$calc$	calculated quantity
f	quantity referred to the air
fit	quantity obtained through fitting process
s	quantity referred to the solid matrix
sp	set-point value for a quantity
w	quantity referred to the overall wall

haust of air through the two parts of the breathing envelope is periodically alternated.

The Breathing Wall technology is thus generally integrated with the HVAC system. In [6] the ventilation requirements are supplied partially through the air permeable envelope and partially through a heat recovery unit, while in [2] the airflow is pre-heated through the breathing roof and then passes through a heat recovery system. It is recognized that the cold airflow across the Breathing Wall can significantly reduce the inner surface temperature, affecting indoor thermal comfort [7]. In order to overcome this problem, some authors [8] recently proposed a new approach, that consists in integrating into the Breathing Wall a capillary water pipes heat exchanger to control inner surface temperature.

From the theoretical point of view, in literature it is possible to find the analytical solution of the steady-periodic problem for a permeable one-layered wall, along with the investigation of the corresponding temperature and heat flux profiles [9]. The solution by Krarti [9] is expressed in terms of non-dimensional numbers, namely Péclet number for the airflow and Biot numbers at the inner and outer wall surface. Subsequent studies addressed the steady state problem for multilayer walls, considering firstly imposed surface temperatures [1], involving then surface thermal resistances [10] and introducing the so-called *dynamic* U-value as a performance parameter for Breathing Walls, to be directly compared with the *static* U-value for conventional walls. When including convection boundary conditions at the wall surfaces, Taylor et al. [10] implicitly assumed that the convection boundary layer is not influenced by the air flow crossing the wall. This assumption has been recently criticized by Craig and Grinham [8], who showed by schlieren imaging and heat flux measurements that a mixed convection boundary layer develops at the Breathing Wall surfaces. Consequently, they found that at the interior surface for increasing air flow velocity a saddle point can be identified, where the convective heat coefficient reaches a minimum. This implies that the surface temperature drop predicted by Taylor and Imbabi might have been underestimated. As far as theoretical models are concerned, recently Ascione et al. [4] developed a finite difference numerical model for a porous wall in transient regime and used the steady state analytical model by Taylor and Imbabi [1] to validate it.

Experimental studies on Breathing Walls in literature are usually devoted to demonstrating the performance of the technology when implemented in real scale buildings and integrated with the HVAC system [5, 11, 12]. Conversely experimental evidences of the validity of the steady state analytical model are rare in literature and refer more to the its consequences than to the model itself. Among them, Taylor and Imbabi [10] used a laboratory apparatus to study the performance of a sample wall made up of mineral wool. The apparatus consisted in a hot box chamber, thermostatically controlled and incorporating the Breathing Wall sample, preceded by an air plenum. Air, whose temperature varied with the laboratory conditions, was pumped into the plenum and forced across the porous wall. The model predictions were verified by checking the dependency of the temperature difference between the wall surfaces and the adjacent air on the airflow rate. Yet the exponential temperature profile into the wall predicted by the model was not reported. Di Giuseppe et al. [13] evaluated the thermal performance of a small prototype of a cellulose based Breathing Wall using a Hot Box test facility, measuring surface temperatures and heat fluxes. Consequently, they focused their attention on the dynamic thermal conductance of the wall as a function of the airflow velocity and did not measure any temperature profile inside the sample. Dimoudi et al. [14] ex-

perimentally investigated, by means of an outdoor test cell facility, the thermal behaviour of a wall component incorporating a Dynamic Insulation technical solution under real weather conditions in Greece. They found a qualitative agreement with the predictions of the analytical model, such as the reduction of the inside surface temperature at increasing airflow rate in contra-flux configuration. Again, they could not verify the temperature profile inside the stratigraphy, since the temperature probes were positioned only at the interfaces between adjacent layers and, moreover, dynamic boundary conditions were applied.

Therefore, to the best of the authors' knowledge, a direct experimental verification of the validity of the steady state analytical model is still lacking. Such a verification can only be obtained by means of a laboratory apparatus allowing to establish steady state boundary conditions on both sides of the porous component. To this purpose a novel laboratory apparatus named Dual Air Vented Thermal Box (DAVTB) was developed by the authors, consisting in a sample wall inserted between a hot and a cold box and an air loop providing the flow rate across it. In the first part of this paper the apparatus and its characteristics are presented. Then the experimental investigation on the steady state behavior of a pervious concrete Breathing Wall at variable airflow rates is reported. A direct verification of the analytical model by Taylor and Imbabi is provided by measuring the temperature profile inside the wall at different positions. From the comparison between theoretical predictions and experimental results the proposal for adjusted boundary conditions for the model is finally derived.

2. Mathematical model

According to the physical approach proposed in all previous works related to the air permeable walls energy behaviour [1, 10], the porous medium is considered isotropic. Moreover, the hypothesis of local thermal equilibrium is introduced. Therefore, quantities are averaged over an elemental volume of the domain, and the resulting energy equation, which takes into account both conduction and advection, becomes [9, 15]:

$$(\rho c)_w \frac{\partial T}{\partial t} + (\rho c_p)_f \nabla \cdot (\mathbf{u}_f T) = \nabla \cdot \lambda_w \nabla T \qquad (1)$$

where T is the temperature distribution, $\mathbf{u}_f$ is the fluid velocity field across the wall (i.e. Darcy velocity), ρ, c and λ are the density, the specific heat (at constant pressure when related to a gas) and the thermal conductivity respectively, referred to the overall porous material (w subscript) or the air only (f subscript). In one dimension and steady state conditions Eq. 1 reduces to [1]:

$$\lambda_w \frac{\mathrm{d}^2 T}{\mathrm{d}x^2} - (\rho c_p)_f u_f \frac{\mathrm{d}T}{\mathrm{d}x} = 0 \qquad (2)$$

The original model in [1] was presented for a three-layers permeable wall with given surface temperatures (Dirichlet boundary conditions). However, for the purpose of this study, the case of a single layer is considered, assuming:

$$\begin{cases} T\,(x = 0) = T_0 \\ \\ T\,(x = L) = T_L \end{cases} \qquad (3)$$

Therefore, defining the model characteristic parameter A as:

$$A = \frac{(\rho c_p)_f u_f}{\lambda_w} \qquad (4)$$

the analytical solution becomes:

$$\frac{T(x) - T_0}{T_L - T_0} = \frac{\mathrm{e}^{Ax} - 1}{\mathrm{e}^{AL} - 1} \qquad (5)$$

where the x axis is directed from outdoor to indoor, leading to positive air velocity when the air flows from outside to inside (contra-flux). As discussed in the Introduction, the effective convective conditions that develop at the Breathing Wall surfaces have been recently investigated by some authors [8], leading to discuss the convective boundary conditions adopted by Taylor and Imbabi [10]. Therefore in this paper the authors chose to focus on the experimental verification of the temperature profile inside the permeable wall, that is the core of the literature analytical model and is independent from the convective heat transfer at the surfaces. Then in this work, the theoretical temperature profile in Eq. 5 is compared to the experimental one referring to a Breathing Wall sample tested in the novel laboratory setup discussed in the following section.

3. Experimental setup

A laboratory setup has been developed in the Building Physics Laboratory of the Energy Department of Politecnico di Milano. It allows to perform experimental analyses on building envelope technologies, both permeable (i.e. Dynamic Insulation) and non-permeable to airflow. A first description of the apparatus was provided in [16], although the control algorithm was at a very preliminary stage.

The objective was to design a relatively small apparatus able to reproduce user-defined operative temperature boundary conditions, both in steady and unsteady state, and, if needed, to force an airflow through permeable components. Due to the latter feature, no useful guideline was found in literature to support the design process: the only technical standard available [17] deals with guarded (GHB) and calibrated (CHB) hotboxes, which are both designed to investigate steady state properties of conventional building envelope components, likewise in [18–20]. In literature, even when Dynamic Insulation walls were involved [10], a basic setup was used, allowing only a partial control of temperature boundary conditions.

The final result of the design process is the Dual Air Vented Thermal Box (*DAVTB*) shown in Figure 1: the apparatus is able to control temperature conditions on both sides of samples, to force an airflow through porous materials, and to reproduce both steady state and dynamic boundary conditions. Therefore, it is also suitable to test other wall technologies, such as cavity walls or PCM-integrated walls, and to investigate their behaviour under unsteady thermal conditions.

The DAVTB facility (Figure 1(a)) is mainly composed by two insulated chambers divided by the sample and connected by the air recirculation system. The operative temperature can be controlled in each chamber separately, using a dedicated heating and cooling plant (Figure 1(b) and 1(c)), and the airflow crossing the sample is controllable in terms of both average velocity and direction. Details about the overall layout and its features are provided in the next sections.

3.1. Chambers

The external dimensions of the chambers are 1.5 m × 1.5 m × 1.29 m each, and their envelope consists of a polystyrene layer, protected by 4 mm laminated panels on both the internal and external side, for a total thickness of 140 mm and an overall conductance of 0.23 W/(m^2·K). The insulated walls minimize the heat flux toward the external environment (laboratory room). The sample is accommodated in a metal frame (1.5 m × 1.5 m) interposed between the chambers. In order to minimize any edge effect and assure one-dimensional heat flux across the sample, the latter is bounded by adequate insulation. The net sample area is thus about 1 m × 1 m. The maximum thickness of the samples that can be tested in the apparatus is 33 cm. The air flows into a chamber and out of the other through two circular openings with a diameter of 20 cm, placed on the back side of each chamber and connected to the airflow loop.

3.2. Heating and cooling plant

As specified above, temperature control inside the chambers is achieved through an hydronic plant, which works both as a heating and cooling system. As shown in Figure 1(c), it is linked to the central supply of the Energy Department building (primary plant) through two water tanks, which provide hot and cold water to the chambers through the secondary plant. As a side note, they also allow to decouple primary and secondary plants for any maintenance operation. Through a preliminary test, the loading time of both tanks has been assessed to be about 3 h, while the maximum and minimum temperatures achievable in the hot and cold tank are found to be 70 °C and 10 °C respectively. Even though water temperature inside the tanks should be fairly stable in order to ensure an effective thermal control, it has been verified that moderate fluctuations do not significantly affect operative and air temperatures inside the chambers.

The secondary plant consists of three parallel water loops: two of them are connected to the radiant panels in each chamber; the third one supplies a water-to-air heat exchanger inside the air recirculation plant. In each loop, supply water temperature to terminals is independently controlled and defined by the user according to the desired thermal conditions: hot and cold water coming from the tanks are mixed in suitable proportion to obtain the desired supply temperature, by acting on two servo-valves for each circuit (a mixing valve and a diverter). Finally, each loop of the secondary plant is equipped with an electric circulation pump.

Dealing with the delivery terminals in the chambers, five radiant panels in parallel are located directly into each box, as shown in Figure 1(b). They are adapted from copper strips for solar collectors. In order to promote the radiative heat exchange toward the sample, all inward surfaces are painted with a matte black varnish, rising the thermal emissivity from 0.01 ÷ 0.07 (typical for non-oxidized copper) to 0.92 ÷ 0.94, assessed by means of thermographic measurement.

3.3. Air recirculation plant

The air recirculation plant is divided into three main sections. The first one is the heat exchanger, mentioned in Subsection 3.2. The second one is the fan section, designed to control the airflow in terms of velocity and direction. It consists of two parallel centrifugal fans facing opposite directions, both equipped with a PWM velocity control (48÷560 Pa at 30.6÷106.2 m^3/h), and two butterfly shutters for each fan. One of the shutters is managed by an ON/OFF controller and is used to insulate one of the circuit branches, while the other is linked

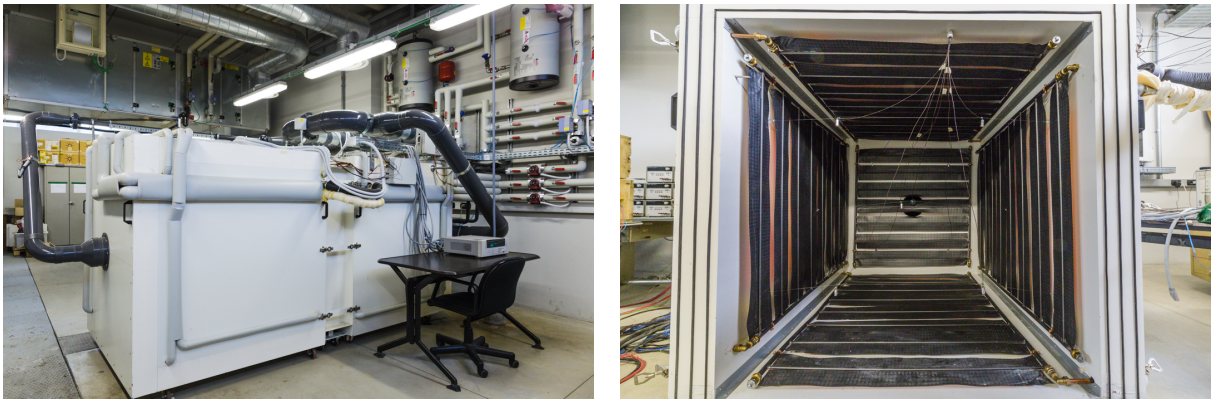

(a) (b)

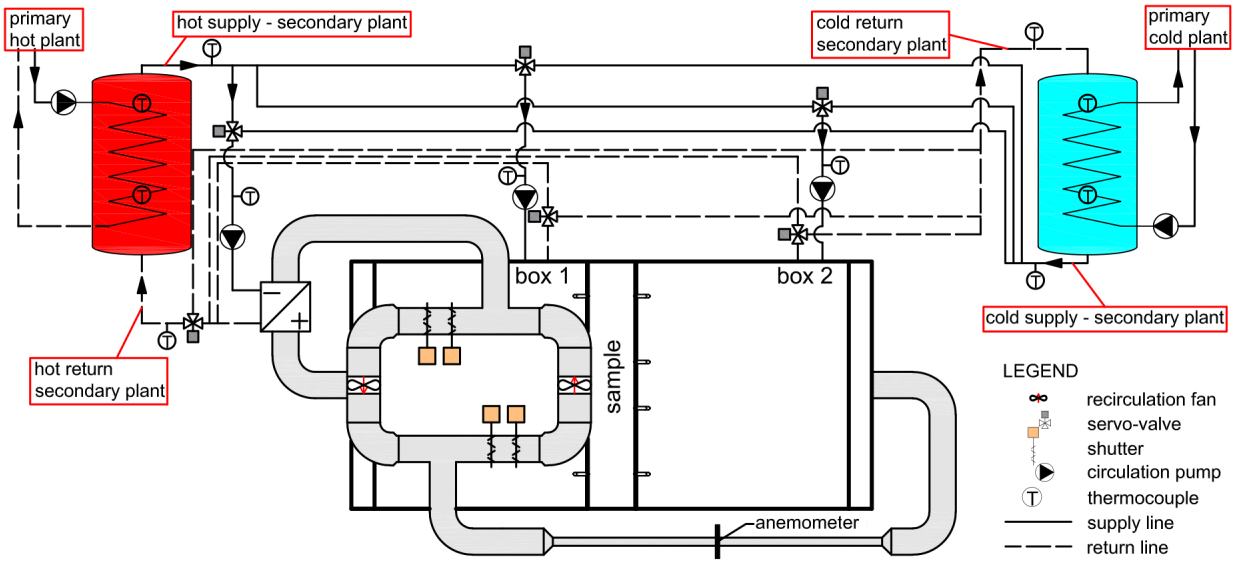

(c)

Figure 1: (a) General view of the DAVTB facility. Box 1 (right) and 2 (left) are visible (with the interposed metal frame to accommodate the sample), along with the hydronic plant and the air recirculation system. (b) Internal view of one of the chambers. Radiant panels and thermocouples are visible. (c) Basic layout of the overall apparatus, with a schematic representation of both hydronic plant and air recirculation system.

to a proportional controller and is aimed at the flow rate fine tuning. The third section of the recirculation system consists of a 2 m long PVC tube (inner diameter 50 mm) and is used to measure the airflow rate, thanks to a small two-directional fan anemometer located in the middle.

Considering the sample investigated in this work, this plant is able to achieve specific airflow rates in the range $0 \div 0.013$ $m^3/(m^2 \cdot s)$, typically suggested by literature as suitable Breathing Wall working conditions [1–7, 12].

3.4. Measurement and control system

Measurement and control in the DAVTB apparatus are carried out by means of a multifunctional switch unit (Agilent 34980A), remotely controlled by a LabVIEW algorithm. The multifunctional switch unit is equipped with three kinds of modules: the first one is used for voltage and current measurement (34921A/T), the second one is a proportional controller and waveform generator (34951A/T), the last one is an ON/OFF controller (34938A/T).

All the electrical devices in the facility (water pumps,

hydraulic valves and butterfly shutters) are activated using the ON/OFF switches. The proportional modules are instead used to regulate mixing valves and diverters to achieve the desired supply temperature to the terminals in the hydraulic plant, to control the proportional shutters in the recirculation plant and, finally, to produce the waveform regulating the rotational velocity of the fans through the PWM controller.

As far as the measurement of environmental parameters is concerned, the following probes have been installed: a bidirectional fan anemometer, a series of thermocouples for air, sample and water temperature measurement and two globe thermometers.

The airflow rate inside the recirculation plant is metered using vane wheel sensor in the measurement section mentioned above (Figure 1(c)). This probe consists of a two-directional fan anemometer measuring velocities in the range $\pm(0.4 \div 20)$ m/s.

All the measurement chain, including the multimeter, the PVC pipe and the fan anemometer, has been calibrated using a reference airflow meter, obtaining a measurement accuracy of $1.3 \cdot 10^{-4}$ m/s.

As far as temperature measurement is concerned, all probes in the DAVTB facility are T-type thermocouples (copper-constantan).

In the hydronic plant water temperature is measured using needle thermocouples. Going more in detail, data are collected in two points of each tank, and in the main locations of every loop of the secondary plant, as shown in Figure 1(c): hot and cold side before the mixing valves, supply to and return from the delivery systems inside the apparatus.

Air temperature is also measured in nine points of each Box at the edges of a cubic arrangement and in the center, allowing the detection of any thermal stratification phenomena. These thermocouples are shielded from the radiative heat exchange by copper sheets. Moreover, a globe thermometer has been installed in the geometrical center to measure the operative temperature. All the mentioned sensors are visible in Figure 1(b).

Finally, it is possible to measure temperature distribution inside the sample at different positions. To this purpose, 55 thermoucouples have been installed in the sample investigated. A more detailed description of their arrangement will be provided in Section 4.

All the aforementioned temperature probes have been calibrated in a temperature range from 0 °C to 70 °C, using a Pt100 resistance thermometer as a reference. This process has led to the definition of a linear calibration equation for each thermocouple. The corresponding correlation errors lie in the interval 0.02 °C÷0.16 °C.

3.5. Temperature control strategy in steady state conditions

Due to the inertial behaviour of the facility, it has been observed that a control logic based on a PID algorithm is not effective in keeping operative temperature sufficiently stable in both chambers, leading to significant temperature errors (up to ±5 °C around the user defined set-point values) and fast discharge of both tanks.

For this reason, a mixed approach has been implemented, based on the combination of a proportional (P) and an ON/OFF controller. The first one, optimized using the Ziegler-Nichols method, allows to achieve the user-defined supply water temperature in the three loops of the secondary plant, by acting on the actuators of mixing valves (a voltage signal in the $0 \div 10$ V range is provided to each one). Event though a simple proportional controller can lead to significant fluctuations of the process variable, it has been observed that brief variations from the desired values do not significantly affect the operative temperature inside the chambers.

In the meantime, the ON/OFF controller reads the process variables (operative temperature for the chambers and air temperature for the heating/cooling battery), calculates their trend and compare it to the corresponding set-point. Their incremental ratio is then calculated, and the future value of the process variable is extrapolated using a response delay (characteristic time t_c) for each loop in the secondary plant. The forecast is then compared to the defined set-point: if the latter is reached or exceeded the corresponding pump is turned OFF, otherwise it keeps working. As far as the characteristic time of the chambers is concerned, it has been defined as the time required to change operative temperature by ±0.1 °C. For the airflow loop, having a negligible inertia compared to the chambers loops, a small characteristic time has been assumed, equal to 30 s. In Table 1, the proportional gain K_p and the characteristic time t_c for each part of the secondary plant are reported. The effectiveness of the present control strategy is discussed in Subsection 5.1.

Table 1: Control parameters.

Parameter	**Box 1**	**Box 2**	**Battery**
K_p $[V/°C]$	0.05	0.05	0.05
t_c $[s]$	100	140	30

It has to be mentioned that at this stage the algorithm is able to reproduce only steady state thermal boundary conditions, while a future development will be the introduction of unsteady boundary conditions.

4. Air permeable concrete and wall sample

In this work, an air permeable wall made of no-fines concrete is experimentally investigated. This material, also known as Air Permeable Concrete (APC) [21], is a cement based mixture produced without using small diameter aggregates. The final result is a highly porous hardened solid matrix, with highly interconnected pores. Among the concrete-based materials and due to its features, no-fines concrete can be considered a suitable choice for Dynamic Insulation technology, in order to develop a multilayer envelope solution optimized for Mediterranean climate conditions in future NZEB applications.

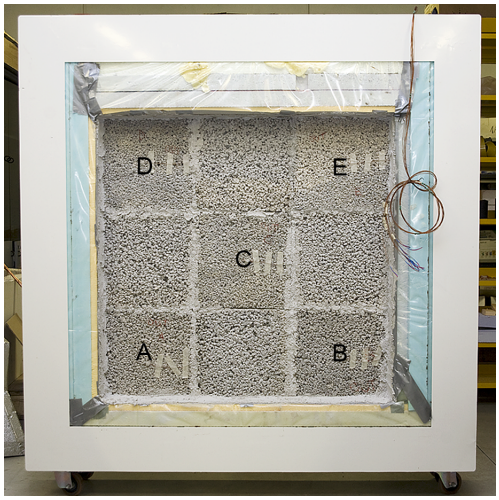

Figure 2: The no-fines concrete wall sample, made up of 9 blocks, accommodated in the metal frame. Thermocouples are embedded in the five blocks labeled from A to E.

The APC wall sample used in this study, with a frontal area of 1 m^2 and a thickness of 15 cm, is shown in Figure 2. Because of its considerable weight, the sample has been divided in 9 elements (32 cm × 32 cm × 15 cm). The temperature distribution along the thickness is measured in 5 blocks (labeled A, B, C, D and E in Figure 2) by means of 9 embedded thermocouples 1.5 cm apart from each other, and 2 thermocouples on the surfaces.

The mix design used for each block is reported in Table 2. The casting procedure has been performed carefully, in order to avoid any damage to the embedded thermocouple junctions. As far as the position of the probes inside the blocks is concerned, it seems reasonable to consider an uncertainty of 2.5 mm introduced by the casting process.

Table 2: Mix design used to cast the no-fines concrete blocks.

cement powder	Portland cement
	CEM II-A-L/42.5
aggregate	Zandobbio limestone
	- 60% large gravel
	ϕ=9÷12 mm
	- 40% medium gravel
	ϕ=6÷9 mm
water/cement ratio (w/c)	0.39
aggregate/cement ratio (agg/c)	7.03

The hardened mixture has then been characterized in terms of thermo-physical properties and structure geometry. First of all, some simplifying assumptions have been introduced to assess the thermal conductivity: the solid-fluid interaction at microscopic level is disregarded and the heat conduction in solid and fluid phases is assumed to occur in parallel [15, 22]. This approach is generally adopted in the literature and leads to consider the thermal conductivity of the porous medium (λ_w) equal to the volume average of the solid and fluid conductivities. Therefore, λ_w is calculated as:

$$\lambda_w = \varepsilon \cdot \lambda_f + (1 - \varepsilon) \cdot \lambda_s \tag{6}$$

where ε is the porosity of the material, while the subscripts f and s are referred to the fluid (air) and the solid phase respectively.

The first step has been the evaluation of the porosity ε. After preparing some dedicated samples with the same features of the Breathing Wall previously described, the Archimedes method was used, as suggested in [21]. The obtained result is ε=(30±2)%.

Then, the thermal conductivity of the solid matrix (λ_s) has been measured directly using the Transient Plane Source (TPS) method [23]. To this purpose, 8 samples have been produced using the same mix-design reported in Table 2, but using only sand and fine gravel (ϕ=1÷2 mm) instead of medium and large aggregates. This has led to very compact specimens ($\varepsilon \approx 0\%$), with the same overall properties of the solid matrix of the no-fines concrete blocks. A series of TPS measurements has shown a solid phase thermal conductivity λ_s equal to (1.76±0.08) W/(m·K).

Considering the outcomes of these two analyses and assuming an air thermal conductivity λ_f=0.025 W/(m·K), that corresponds to a temperature of 15 °C, through Eq. 6 the average thermal conductivity of the porous material was calculated as λ_w=(1.24±0.09) W/(m·K).

5. Results and discussion

The wall sample described in Section 4 has been tested in contra-flux conditions, by setting an operative temperature equal to 15 °C in Box 1 and 40 °C in Box 2. In this way, it has been possible to achieve an overall temperature difference of 25 °C, which is representative for winter design conditions in Italy. It is important to notice that, since no phase change material or second order phenomena are involved in this study, the only relevant parameter is the temperature difference between indoor and outdoor, while the absolute temperature values are less important. As far as the airflow rate is concerned, six conditions have been investigated: first of all, a null velocity case is considered, in which the sample behaves as a traditional non-permeable wall. Then, five incremental levels of airflow rate were reproduced, leading to average air velocities equal to 0.001 m/s, 0.003 m/s, 0.006 m/s, 0.009 m/s and 0.012 m/s.

The effectiveness of the control strategy developed for the DAVTB apparatus is discussed below. Then, the outcomes of the experimental tests performed are compared to the analytical model for single layer Breathing Walls under steady state Dirichlet boundary conditions. To this extent, the velocity of the air flowing through the porous material is finally analyzed and discussed in detail.

5.1. Stability of thermal boundary conditions

Due to changes in airflow rate crossing the sample from a Box to the other, the energy need related to the temperature control in each chamber changes in every test, leading to different values of the water supply temperature. Therefore, the first step has been the evaluation of the thermal stability in both chambers. To this extent the control error $E(t)$ can be introduced as:

$$E(t) = T_{sp} - T(t) \tag{7}$$

where T_{sp} is the desired temperature value and $T(t)$ is the corresponding measured value. According to Eq. 7, measured values greater then the set-point give negative control errors, while measured temperatures below the desired value lead to positive $E(t)$. This quantity has been calculated considering operative temperature of both chambers and their difference $(T_1 - T_2)$. The resulting frequency distributions are reported in Figure 3 for each test performed. It is possible to notice that the control error fluctuation is always in the range ±0.3 °C, and is generally centered around the 0 °C value.

In Table 3 for every performed test the thermal conditions in Box 1 and 2 are reported, in terms of average and mean quadratic error σ calculated neglecting the initial transient period. Mean quadratic errors are generally lower than 0.1 °C and thus the control strategy adopted appears effective.

Table 3: Average and standard deviation of the temperature conditions achieved in each test performed.

ID	$\langle \mathbf{u} \rangle$	$\mathbf{T_1}$	σ_1	$\mathbf{T_2}$	σ_2	$\mathbf{\Delta T}$	$\sigma_{\Delta T}$
	[m/s]	[°C]	[°C]	[°C]	[°C]	[°C]	[°C]
1	0	15.03	0.05	39.96	0.04	24.94	0.06
2	0.001	15.00	0.07	39.96	0.05	24.96	0.09
3	0.003	15.02	0.04	39.94	0.03	24.92	0.05
4	0.006	14.96	0.06	39.95	0.04	24.99	0.07
5	0.009	14.97	0.06	39.94	0.05	24.97	0.08
6	0.012	14.98	0.05	39.93	0.04	24.94	0.06

Therefore, it is possible to assess the ability of the control algorithm to provide stable operative temperatures and to effectively reproduce the steady state condition investigated in this work.

5.2. Comparison between analytical and measured temperature profiles

During every test, the temperature distribution across all the five blocks in the air permeable sample has been measured. As stated in Section 4, for each block 11 thermocouples are arranged and their readings are collected every 5 s. All tests lasted at least two days and instantaneous temperature values have been time-averaged once steady state has been reached. It takes in fact 1 h to achieve the desired operative temperature values in both chambers, while steady state can be observed in the sample after 11÷18 h, depending on the crossing airflow velocity. Results are then compared with the corresponding analytical curve calculated using Eq. 5, with the only exception of the first test in which the sample is not crossed by the airflow and a linear temperature distribution is expected.

As far as tests 2 to 6 are concerned, the A parameter has been calculated according to Eq. 4 (A_{calc}), by adopting air properties at the entering section temperature of 15 °C (density 1.23 kg/m^3, specific heat capacity at constant pressure 1004.9 J/(kg·K), thermal conductivity 0.025 W/(m·K)), thermal conductivity of the porous wall equal to 1.24 W/(m·K) as derived in Section 4, and air velocity as the average from measurements at regime.

In Figure 4 experimental results are compared to the corresponding analytical curve in block C, which is located in the central part of the sample and therefore not affected by edge effects (Figure 2). It is possible to observe that the deviation from the linear trend increases

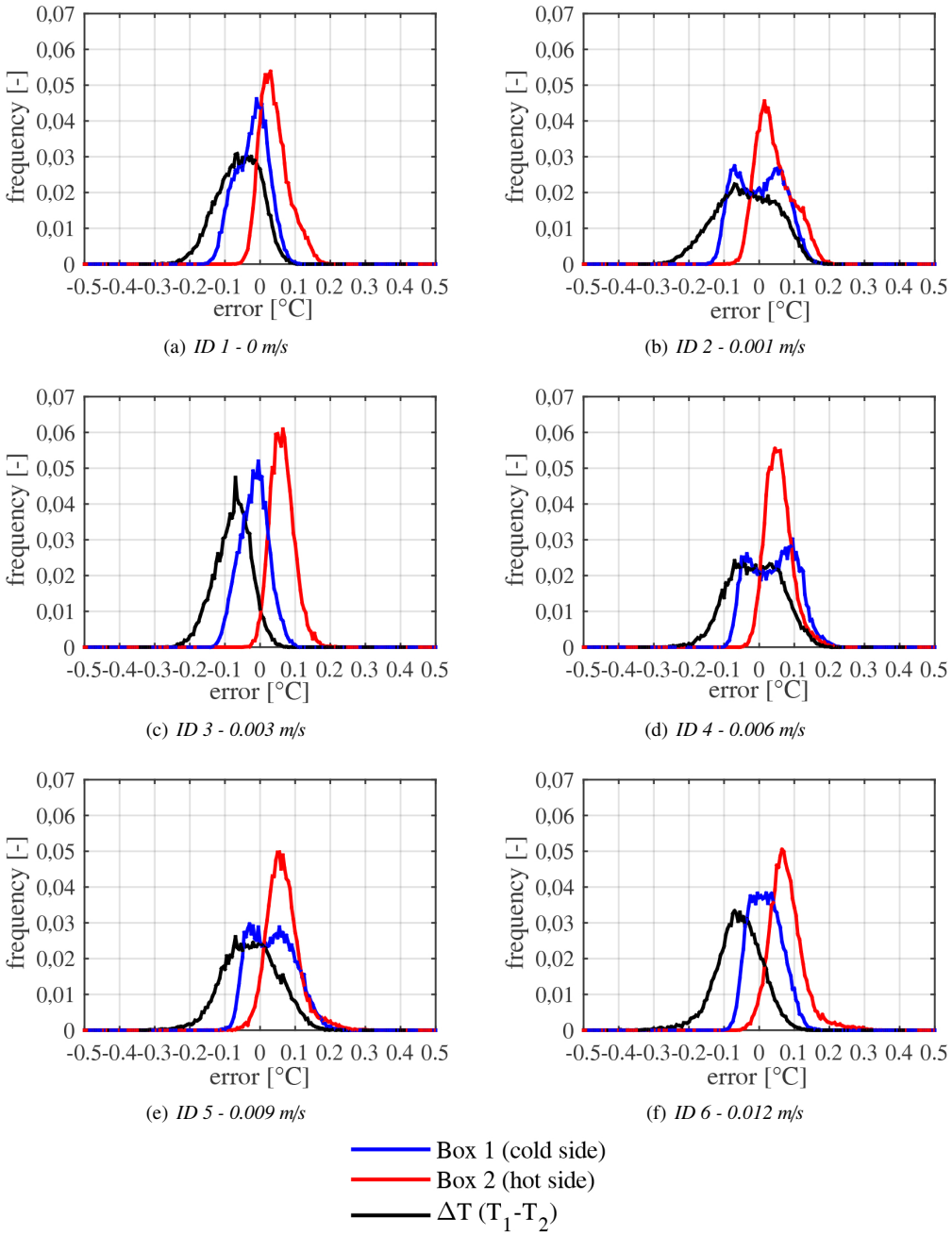

(a) *ID 1 - 0 m/s*

(b) *ID 2 - 0.001 m/s*

(c) *ID 3 - 0.003 m/s*

(d) *ID 4 - 0.006 m/s*

(e) *ID 5 - 0.009 m/s*

(f) *ID 6 - 0.012 m/s*

Figure 3: Frequency distribution of control errors related to operative temperature in Box 1 and 2, and their difference, for the various air velocity regimes investigated: (a) 0 m/s, (b) 0.001 m/s, (c) 0.003 m/s, (d) 0.006 m/s, (e) 0.009 m/s and (f) 0.012 m/s.

with the air velocity. Moreover, the analytical model described in Eq. 5 reproduces with good accuracy the outcomes from the measurements: indeed, the mean standard deviations between the calculated and the corresponding measured values are 0.20 °C, 0.15 °C, 0.11 °C, 0.16 °C and 0.12 °C for tests from 2 to 6. This result is also an indirect confirmation of the reliability of the thermal conductivity measured through TPS for the no-fines concrete solid matrix.

Figure 4 provides also a qualitative confirmation of

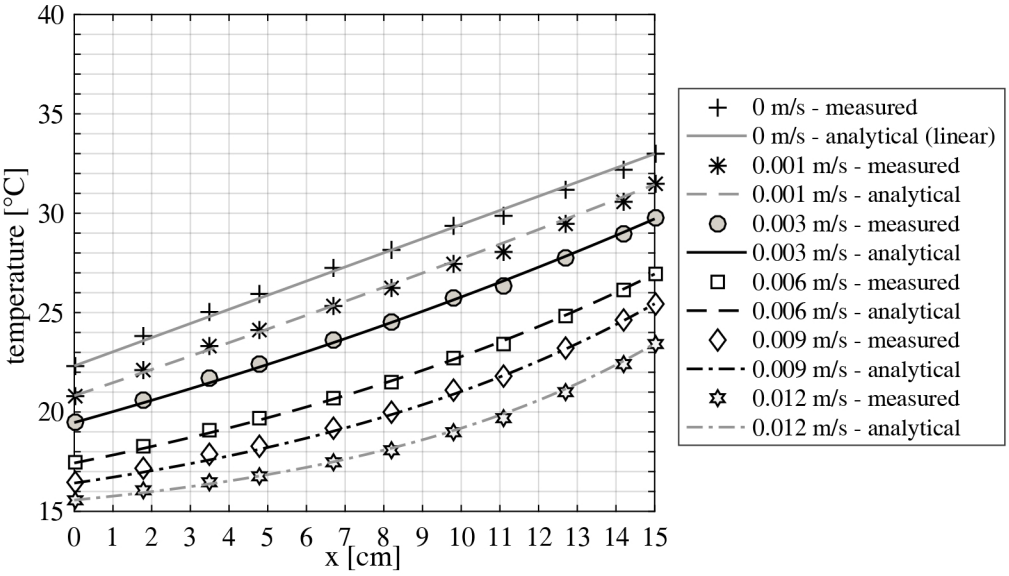

Figure 4: Measured and calculated temperature profile across the C block inside the wall sample at various air velocities.

the thermo-physical behaviour depicted by the analytical model based on convective-radiative boundary conditions, namely the temperature drop on both surfaces of the Breathing Wall in contra-flux regime, as reported in [9, 10]. This phenomenon is clearly visible in the results of the laboratory tests performed. In [8] Craig and Grinham quantitatively compare the Nusselt number (Nu_m) on the surface of a Breathing Wall sample crossed by an airflow to the Nusselt number referred to natural convection on a vertical surface (Nu_n) and represent the ratio Nu_m/Nu_n as a function of the ratio $\sqrt{Pe}/Nu_n$. Following the methodology reported in [8], it has been found that at our working conditions the ratio $\sqrt{Pe}/Nu_n$ lies in the range $0.12 \div 0.33$, that leads to a ratio Nu_m/Nu_n dropping from 0.98 to 0.62. This means that increasing the airflow velocity from 0 m/s to 0.012 m/s, the convective heat transfer coefficient related to the wall surface toward Box 2 decreases by 38%. Consequently, the effectiveness of convection as a mechanism to heat the sample is reduced, causing the observed surface temperature drop. At the same time, at the highest velocity considered (0.012 m/s) the wall exterior surface temperature (facing the cold chamber) almost reaches the asymptotic value of 15 °C, equal to the operative temperature in Box 1.

As a next step, the temperature profile across the Breathing Wall has been studied also in the other blocks, namely A and B at the bottom of the wall, D and E on the top. This would provide a further confirmation of the analytical model, but also more details about the overall behaviour of the experimental setup.

In Figure 5 the temperature profiles across the five blocks, obtained in the same way as for block C, are reported for all the six tests performed. First of all, at every airflow velocity, a temperature stratification in both chambers, likely due to natural convection phenomena, can be remarked. Blocks A and B show generally lower surface temperatures than blocks D and E, both on cold and hot side, with block C temperatures in between. This outcome provides additional reasons to compare measurements with the analytical model based on Dirichlet boundary conditions, rather than on convective-radiative flux conditions. Actually, in the latter case each block would be characterized either by a local operative temperature or by a local surface resistance, whose determination is not straightforward. At the same time it can be noticed that temperature profiles corresponding to blocks at the same height are not always coherent, especially for the top blocks D and E. This finding can be explained by local non-uniformity of the radiant panels in the hydraulic heating and cooling plant, caused by its layout (i.e. location of delivery and return sections).

Moreover, even though the agreement with the temperature profiles calculated using Eq. 5 and A_{calc} is still acceptable, as shown in Table 4, the discrepancy between measured and calculated data becomes noticeable both on the top and on the bottom of the Breathing Wall sample.

Local deviations cannot be attributed to differences in thermo-physical and microstructural properties, since all blocks have been produced in the same way and at

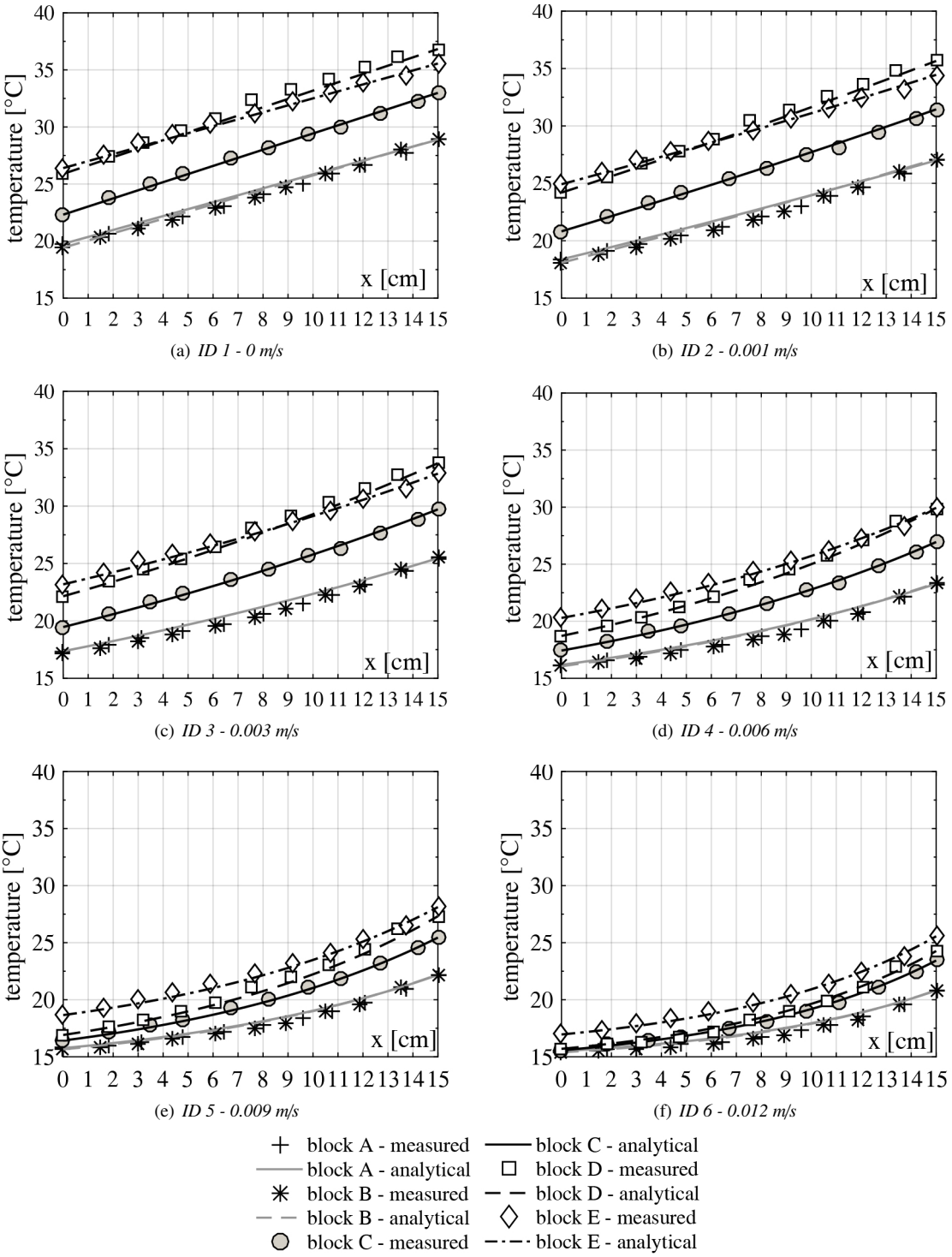

Figure 5: Measured and calculated temperature profiles across the five blocks of the sample wall, for the various air velocities investigated: (a) 0 m/s, (b) 0.001 m/s, (c) 0.003 m/s, (d) 0.006 m/s, (e) 0.009 m/s and (f) 0.012 m/s.

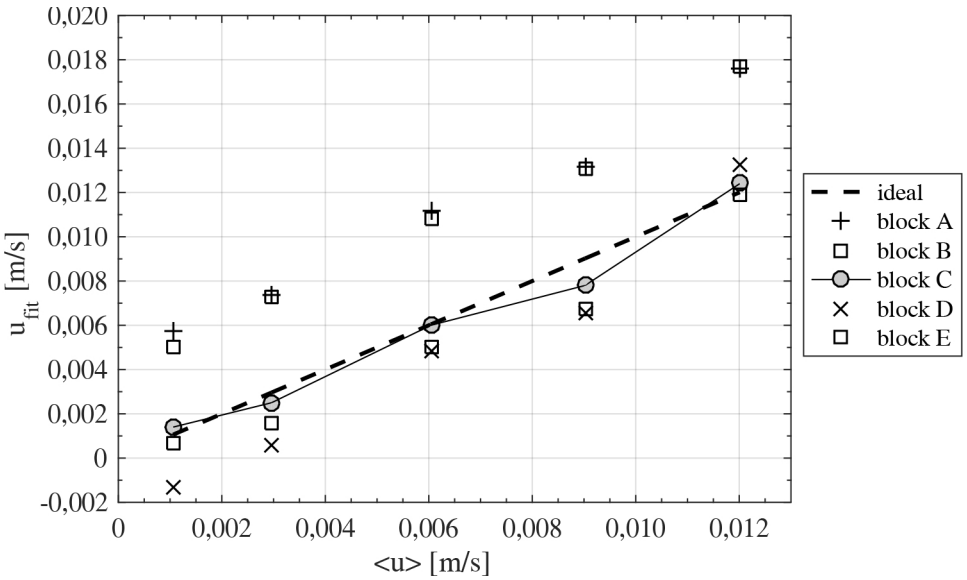

Figure 6: Fitting-derived velocity (u_{fit})versus average expected velocity $\langle u \rangle$ for each block of the wall sample.

Table 4: Mean standard deviation between measured and calculated temperature profiles for each block at different air velocities.

ID	⟨u⟩	A	B	C	D	E
	[m/s]	[°C]	[°C]	[°C]	[°C]	[°C]
2	0.001	0.54	0.47	0.20	0.43	0.18
3	0.003	0.48	0.47	0.15	0.46	0.24
4	0.006	0.47	0.47	0.11	0.34	0.23
5	0.009	0.34	0.34	0.16	0.43	0.33
6	0.012	0.38	0.38	0.12	0.25	0.18

the same time. Moreover, since the analytical model is based on Dirichlet boundary conditions, the vertical stratification in temperature does not have any effect. These two considerations lead to suppose a non uniform velocity field on the wall inlet surface.

5.3. Air velocity distribution on the sample surface

Indeed, the airflow rate is measured in a dedicated section of the recirculation plant (Figure 1(c)). Then the average velocity is calculated considering a uniform distribution over the entire sample surface (1 m^2), since it is not technically straightforward to obtain a direct measurement of the local velocity distribution.

In order to obtain a prediction of the velocity variation in the various parts of the sample, measured temperature profiles have been fitted with Eq. 5, considering A as the fitting parameter. The obtained values A_{fit} have then been used to derive through Eq. 4 a corresponding velocity value (u_{fit}). This value is compared to the corresponding average measured value $\langle u \rangle$, which implies a uniform velocity field on the overall sample surface. Results are shown in Figure 6, where the *ideal* line (dotted) represents the perfect agreement between the expected value $\langle u \rangle$ and the corresponding result of the fitting process u_{fit}.

Figure 6 shows that blocks on the lower part of the sample (A and B) are affected by crossing air velocity generally higher than the average value, while the topmost parts of the Breathing Wall (blocks D and E) are characterized by opposite conditions. Block C, located in the very center of the wall, shows a generally good agreement between $\langle u \rangle$ and u_{fit}. Moreover, blocks D and E show again a different behaviour, as previously noted about the temperature profile.

In order to explain these outcomes, it has to be remarked that the sample surfaces exchange heat with each box both by radiation with the surrounding surfaces and by convection with the air. As far as convection is concerned, since in each chamber the sample surface temperature is different from the other surfaces, a buoyancy driven air circulation can be expected. Considering the actual temperature distribution, the circulation in cold Box 1 should be characterized by air lifting next to the warm sample surface and dropping in the back of the chamber. An opposite flow (ascendent on the back of the chamber and dropping next to the sample surface) can be expected in hot Box 2. This air movement should then generate an additional pressure difference across the sample, varying from the bottom to the top of the experimental setup and affecting the

forced airflow through the Breathing Wall. Therefore, a mixed convection regime around the Breathing Walls can be expected, resulting from the combined forced airflow across the sample and the room-scale natural convection in each box. A similar mixed convection condition for the permeable sample has been recently highlighted by Craig and Grinham [8], although in their experiment natural convection derived from bouyancy forces on a vertical plate. According to [8], when the superficial temperature is below the ambient temperature an increased airflow should be expected at the bottom of the sample, such as what is reported in Figure 6.

In order to verify this hypothesis in qualitative terms, a series of 2D CFD simulations in ANSYS Fluent has been performed. In a first step, Box 1 and 2 have been simulated separately as two closed chambers, neglecting both the air permeability of the porous sample in between and the presence of inlet and outlet sections. This way a rough estimation of the order of magnitude of air movement inside both chambers due only to natural convection has been derived. Secondly, the entire apparatus has been treated in a single simulation, introducing the porous sub-domain describing the Breathing Wall sample.

As far as the modeling process is concerned, in both steps a simplified two-dimensional geometry has been used, neglecting all complexities related to the radiant panels. Spatial discretization has been done with a structured quadrilateral mesh, with an orthogonal grid quality of 1, skewness of 0 and an aspect ratio of approximately 1.146 [24]. Calculations are performed in double precision, and the solution methods used are the SIMPLE scheme for the pressure-velocity coupling, second order and second order upwind for the spatial discretization in all the governing equations. All boundary conditions are based on the data collected during test 6, being the case where forced flow is maximum. For the first simplified simulations the following boundary conditions have been assumed:

1. surface temperature of cooled walls in Box 1 equal to 13.5 °C (average between supply and return water in the cooling plant);
2. surface temperature of heated walls in Box 2 equal to 47.5 °C (average between supply and return water in the heating plant);
3. surface temperature of sample in Box 1 equal to 15.8 °C, derived from measurements;
4. surface temperature of sample in Box 2 equal to 23.0 °C, derived from measurements.

As far as the second step simulation is regarded, boundary conditions 1) and 2) have been maintained, while conditions 3) and 4) could not be set because the sample surfaces are inside the domain. In turn, an inlet volume airflow rate of 0.012 m^3/s in Box 1 has been adopted, at a temperature of 15.0 °C (derived from measurements), with a turbulence intensity of 6.94% and a hydraulic diameter of 0.2 m (both defined according to [24]). In both simulations (separate Boxes and overall apparatus) energy equations have been solved, turbulence has been taken into account using a realizable $k - \varepsilon$ model, with enhanced wall treatment and the activation of buoyancy effect in the transport equation for ε, and air density has been calculated as a function of temperature using the Boussinesq model. As convergence criteria, it has been verified that residuals have dropped below 10^{-10} for energy and 10^{-6} for other quantities, and that they showed a decreasing trend.

Moreover, in the complete apparatus simulation performed in the second step, the porous domain model has been introduced to simulate the no-fines concrete sample. It is important to underline that this approach treats the porous part of the domain as a fluid material with peculiar features, such as porosity (which affects the average thermal conductivity likewise Eq. 6) and air permeability. On the other hand, this means that the interfaces between the porous and the fluid subdomains are only virtual, and superficial heat transfer (either convective or radiative) can not be treated properly. Also for this reason the results of this simulation have to be considered qualitatively.

In Figure 7 the most relevant outcomes of the CFD analysis are displayed: in Figure 7(a) the pressure distribution obtained from the separate simulation of Box 1 and 2 is shown along with the air velocity field, while in Figure 7(b) the same quantities are referred to the simulation of the whole apparatus, including the porous wall.

In the first simulation, it is possible to observe that the air motion activated by the buoyancy flow alone behaves as previously postulated. Therefore, since in test 6 air should move across the sample from Box 1 to Box 2, the vertical pressure gradient caused by the natural convection phenomena depicted in Figure 7(a) would lead to a pressure difference variable along the vertical direction, causing local deviations of fluid velocity from the expected value of 0.012 m/s coherent with the behaviour shown in Figure 6.

The simulation of the complete apparatus leads to comparable results: in Figure 7(b) it is possible to observe a mixed convection condition, where a recirculation phenomenon similar to that discussed above gives a comparable displacement of the pressure distribution. Again, it is possible to observe a pressure difference across the sample varying from the top to the bottom,

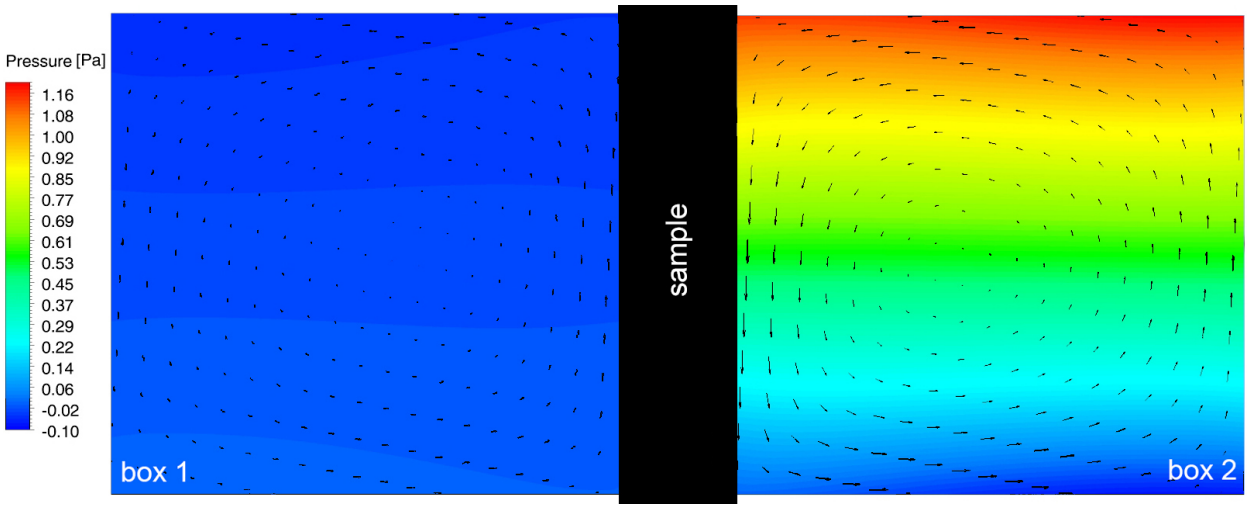

(a)

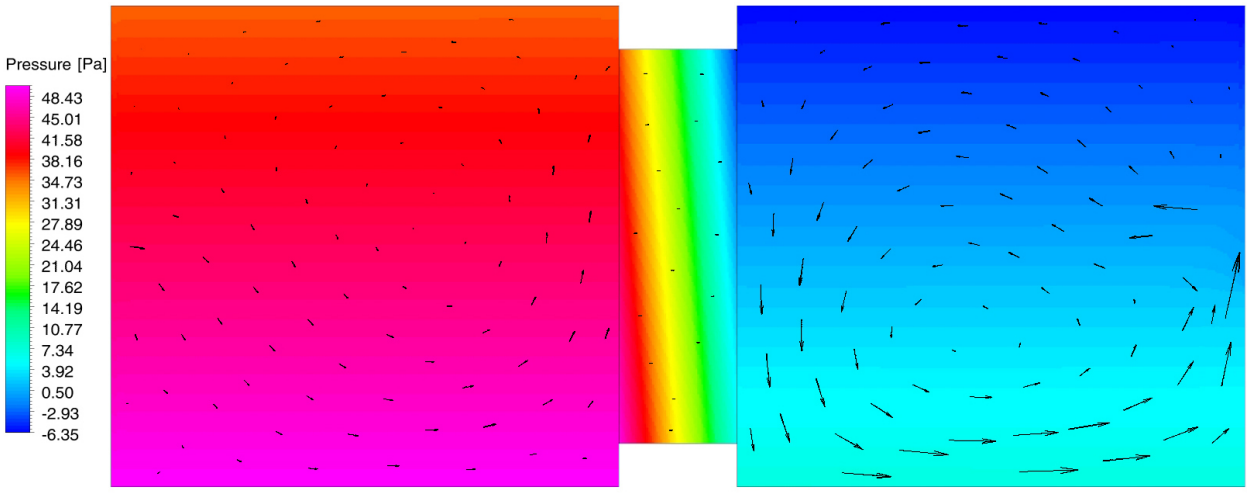

(b)

Figure 7: (a) Pressure distribution inside Box 1 and Box 2 calculated through CFD simulation of both chambers separately, where sample air permeability is neglected. Velocity fields in both boxes are shown through black arrows (in Box 1 they are scaled up five times for visibility purpose). (b) Pressure distribution inside the entire apparatus calculated through CFD simulation with the introduction of the porous domain to describe the sample. Velocity field is shown through black arrows.

even though the magnitude of this trend is mitigated by the permeability of the porous domain, in comparison to what can be inferred by Figure 7(a). The resulting air velocity distribution along the sample surface is again coherent with Figure 6, with smaller values on the top (where the air motion due to natural convection is in opposition to that provided by forced convection) and bigger values on the bottom (where the air motion caused by the recirculation plant is increased by the pressure difference generated by the buoyancy flow in both chambers). This behaviour is also summarized in Figure 8, which provides a representation of the vertical distribution of both non-dimensional pressure difference between the sample faces and non-dimensional airflow velocity across the Breathing Wall, derived from the overall apparatus CFD simulation.

Finally, the outcomes of the CFD analysis presented above provide a qualitative proof that a non-uniform air velocity on the sample, which has been inferred as a result of the fitting process previously described, can be explained in terms of a mixed convection regime throughout the experimental apparatus due to the Boxes

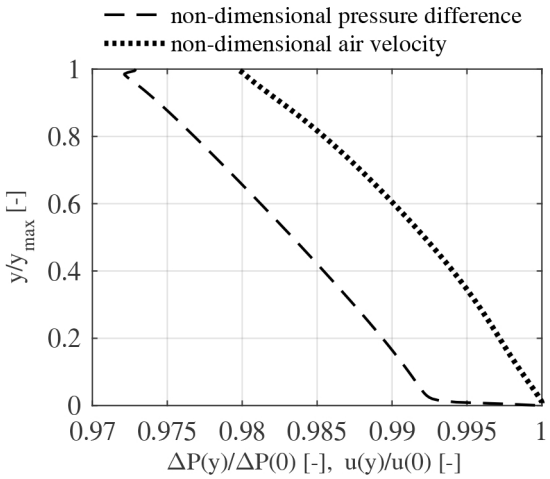

Figure 8: Vertical distribution of non-dimensional velocity and non-dimensional pressure difference across the sample. Results come from the CFD simulation of the overall apparatus.

small size and the features of the delivery terminals.

6. Conclusions

The main focus of this work was to experimentally investigate the validity of the analytical model for the temperature profile inside Breathing Walls under steady state Dirichlet boundary condition, provided by [1]. This was made possible by the development of a novel apparatus named DAVTB, which was used to study an APC wall.

In the first part of this paper, the novel DAVTB apparatus was presented. The effectiveness of the mixed proportional and ON/OFF control algorithm used to obtain the desired operative temperature conditions was assessed: the system is able to reach the set-point thermal conditions at every airflow velocity level and the operative temperature are sufficiently stable to replicate the ideal steady state condition. Indeed, frequency distribution of instantaneous temperature deviations always falls within the range ±0.3 °C, while the average deviation between measured and desired values is always in the range ±0.1 °C.

Then the no-fines concrete material used in the Breathing Wall under study was experimentally characterized in terms of average porosity ε=30±2% and thermal conductivity of the solid matrix λ_s=1.76±0.08 W/(m·K). Staring from these quantities, an overall thermal conductivity of the porous material of 1.24±0.09 W/(m·K) was assessed.

The experimental campaign consisted of six tests, all performed imposing a 25 °C temperature difference between the two chambers of the laboratory setup (T_1=15 °C and T_2=40 °C), with six different values of the airflow velocity across the wall sample: a first one with no airflow, and five more in contra-flux regime from 0.001 m/s to 0.012 m/s. Temperature profile across the specimen was measured in five positions, and collected data were directly compared to the corresponding theoretical curve.

Experimental evidences show a generally good agreement between calculated and measured temperature distribution, especially focusing on the centermost part of the sample (block C), where the mean standard deviation between experimental and analytical values was in the range 0.11 °C÷0.20 °C. The typical exponential trend was clearly visible in all parts of the Breathing Wall, along with the surface temperature drop at increasing air velocity.

However, the fitting process of the measured data has shown that the velocity field at the wall inlet is not as uniform as expected, because of a mixed convection condition that shows some similarities to the one recently investigated by some authors [8]. This hypothesis has been qualitatively verified by means of CFD simulations of simple two-dimensional geometries representing the DAVTB apparatus. The simulation outcomes have confirmed that, due to recirculating phenomena driven by natural convection and to the very low forced flow velocity typical of Breathing Walls applications, the pressure gradient across the sample changes from the top to the bottom of the wall itself, leading to velocities that decreases with height. Although the specific velocity field across the Breathing Wall under study clearly depends on the geometry of the chambers and on the air circulation system in the apparatus, these outcomes allow to derive some general considerations about the applicability of the theoretical model. Depending on the layout of the air circulation system adopted in a Breathing Wall, a velocity field will develop at the wall inlet. Such field is likely to influence the local and then the overall Breathing Wall performance. The only way to take the velocity field into account within the one-dimensional analytical model is thus to adopt two or three-dimensional velocity boundary conditions. Such adjusted boundary conditions may derive from CFD or simplified Air Flow Networks calculations.

Future developments of this work include the definition of a control algorithm suitable to reproduce unsteady state boundary conditions in the DAVTB apparatus. Then, the no-fines concrete sample discussed

in this work will be investigated under dynamic conditions, and measured values will be compared to a suitable finite difference based numerical model. At the same time, the characterization of the Air Permeable Concrete will be completed, in terms of both thermophysical properties and micro-structural geometry, and the macroscopic effects of the thermal interactions between solid and fluid phase at microscopic level will be investigated.

Funding

This research did not receive any specific grant from funding agencies in the public, commercial, or not-for-profit sectors.

References

[1] B.J. Taylor, D.A. Cawthorne, M.S. Imbabi, Analytical investigation of the steady-state behaviour of dynamic and diffusive building envelopes. Building and Environment 31 (1996) 519-525.

[2] M.S. Imbabi, A.R. Brown, A. Peacock, J. Murphy, The transforming technology of dynamic breathing building, Proceedings Ecocity World Summit San Francisco USA (2008) 1-12.

[3] B.J. Taylor, R. Webster, M.S. Imbabi, The building envelope as an air filter. Building and Environment 34 (1999) 353-361.

[4] F. Ascione, N. Bianco, C. De Stasio, G.M. Mauro, G.P. Vanoli, Dynamic insulation of the building envelope: Numerical modeling under transient conditions and coupling with nocturnal free cooling. Applied Thermal Engineering 84 (2015) 1-14.

[5] S. Murata, T. Tsukidate, A. Fukushima, M. Abuku,H. Watanabe,A. Ogawa, Periodic alternation between intake and exhaust of air in dynamic insulation: measurements of heat and moisture recovery efficiency. Energy Procedia 78 (2015) 531-536.

[6] B.J. Taylor, M.S. Imbabi, The application of dynamic insulation in buildings. Renewable Energy 15 (1998) 377-382.

[7] G. Gan, Numerical evaluation of thermal comfort in rooms with dynamic insulation, Building and Environment 35 (2000) 445-453.

[8] S. Craig, J. Grinham, Breathing walls: The design of porous materials for heat exchange and decentralized ventilation. Energy and Building 149 (2017) 246-259.

[9] M. Krarti, Effect of air flow on heat transfer in walls. Journal of Solar Energy Engineering 116 (1994) 35-42.

[10] B.J. Taylor, M.S. Imbabi, The effect of air film thermal resistance on the behaviour of dynamic insulation. Building and Environment 32 (1997) 397-404.

[11] A. Rainy Brown, M.Imbabi, A. Peacock, The Balerno Project. Proceedings of the X World Renewable Energy Congress, Glasgow, UK (2008).

[12] E. Elsarrag, Y. Al-Horr, M.S. Imbabi, Improving building fabric energy efficiency in hot humid climates using dynamic insulation, Building Simulation 5, 2 (2012) 127-134.

[13] E. Di Giuseppe, M. D'Orazio, C. Di Perna, Thermal and filtration performance assessment of a dynamic insulation system. Energy Procedia 78 (2015) 513-518.

[14] A. Dimoudi, A. Androutsopoulos, S. Lykoudis, Experimental work on a linked, dynamic and ventilated wall component. Energy and Building 36 (2004) 443-453.

[15] D.A. Nield, A. Bejan, Convection in Porous Media. 3^{rd} edition. USA, Springer (2000).

[16] A. Alongi, L. Mazzarella, The Dual Air Vented Thermal Box: a laboratory apparatus to test air permeable building envelope technologies. Energy Procedia 78 (2015) 1543-1548.

[17] UNI EN ISO 8990, Thermal insulation. Determination of steady-state thermal transmission properties. Calibrated and guarded hot-box. Ente Italiano di Unificazione, Milano, 1996.

[18] A. Ghosh, S. Ghosh, S. Neogi, Performance evaluation of a guarded hot box U-value measurement facility under different software based temperature control strategies. Energy Procedia 54 (2014) 448-454.

[19] K. Martin, I. Flores, C. Escudero, A. Apaolaza, J.M. Sala, Methodology for the calculation of response factors through experimental tests and validation with simulation. Energy and Buildings 42 (2010) 461-467.

[20] F. Asdrubali, G. Baldinelli, Thermal transmittance measurements with the hot box method: Calibration, experimental procedures, and uncertainty analyses of three different approaches. Energy and Buildings 43 (2011) 1618-1626.

[21] J.M. Wong, F.P. Glasser, M.S. Imbabi, Evaluation of thermal conductivity in air permeable concrete for dynamic breathing wall construction. Cement & Concrete Composites 29 (2007) 647-655.

[22] M. Kaviany, Principle of Heat Transfer in Porous Media. 2^{nd} edition. New York, Springer (1995).

[23] Y. He, Rapid thermal conductivity measurement with a hot disk sensor - part 1. Theoretical considerations. Thermochimica Acta 436 (2005) 122-129.

[24] ANSYS, ANSYS FLUENT 17.1 - User's guide. Pittsburgh, ANSYS Inc. (2016).